Accepted manuscript. Published in Geotechnique Letters (2026). Version of record: https://doi.org/10.1680/jgele.24.00153. This is the authors' final version after peer review. Please cite the published article.

Long-term Creep and Permeability Evolution of Tailings Sand at Elevated Stresses

Shubjot Singh[1], Yuxuan Wen[2], Wanqi Yu[3], Efraín Rondinel[4], Julie A. Korak[5], Giuseppe Buscarnera[6], Yida Zhang[7*]

ABSTRACT

Tailings dams are typically constructed utilizing the coarser fraction of tailings and are engineered to contain the finer fraction of the waste. For extremely tall tailings dams, the high internal stress near the bottom of the dam may induce particle breakage in the embankment material (coarser fraction), resulting in an increase in fines content. This can further lead to reduced hydraulic conductivity, raised water level, and endanger the stability of the dam. Another often neglected aspect is that grain crushing may not happen instantaneously at the moment of the application of the load but develop gradually over time due to delayed crack growth (or static fatigue) within the grains, even at relatively intermediate or low stress levels. Considering the expected long service life (50-100 years) of typical tailings storage facilities (TSF), it is critical to quantify the degree of grain breakage and the induced creep and permeability reduction under sustained stresses over extended period of times. We conducted a 450-day long creep test on tailings sand retrieved from a currently active TSF at in-situ vertical stress (3 MPa) using a custom-built high-stress-permeability (HSP) oedometer cell. The experiment shows a clear change in vertical strain and hydraulic conductivity, with hydraulic conductivity steadily declining during the creep stage before reaching a stable value. The results are subsequently interpreted by combining a rate-dependent breakage mechanics model which tracks the evolution of grain size distribution over time and several hydraulic conductivity models that account for both porosity and grain size effects. The model predictions generally agree well with the experimental data. Finally, possible sources of discrepancies and recommendations for future long-term creep tests on tailings materials are discussed.

Keywords: High-stress compression; Creep; Grain breakage; Permeability; Tailings

[1] Ph.D. student, Dept. of Civil and Environ. Eng., Northwestern University, Evanston, IL, 60208
[2] Postdoctoral Scholar, School of Civil and Construction Eng., Oregon State University, Corvallis, OR, 97331.
[3] Graduate student, Dept. of Civil, Environ. and Architect. Eng., University of Colorado Boulder, Boulder, CO, 80309.
[4] Tailings and Waste Discipline Leader, Stantec, Lima, Perú, 15073.
[5] Assistant Professor, Dept. of Civil, Environ. and Architect. Eng., University of Colorado Boulder, Boulder, CO, 80309.
[6] Professor, Dept. of Civil and Environ. Eng., Northwestern University, Evanston, IL, 60208.
[7]* Associate Professor, Dept. of Civil, Environ. and Architect. Eng., University of Colorado Boulder, Boulder, CO, 80309. Email: yida.zhang@colorado.edu

INTRODUCTION

Recent catastrophic failures of large dams without obvious external triggers (Santamarina *et al.* 2019) highlight the critical need for better characterizing the gradual evolution of soil properties and assessing its impact on the overall stability of critical geo-structures throughout their service lives. For tailings dams, the sand used for construction is restricted to a fines content of less than 15% (Barrera *et al.* 2011; Valenzuela 2016) to ensure adequate drainage and minimizing the risk of liquefaction. However, raising embankment heights and hence increasing overburden stresses can lead to gradual grain breakage and fines generation at the dam base. Riemer *et al.* (2008) documented a 5-6% increase in fines content by increasing the confining pressure from 0 to 5.5 MPa. Singh *et al.* (2021) showed that increasing the vertical stress from 5 to 40 MPa under oedometric conditions reduces the hydraulic conductivity of tailings sand by tenfold.

In addition to immediate crushing in response to a stress increase, particle breakage can occur overtime even under constant stress (Leung *et al.* 1996). Short-term creep and relaxation tests lasting up to 24 hours have shown that the time-dependent response of granular soils is primarily governed by the delayed breakage of individual particles and the subsequent rearrangement of soil skeleton over time (Takei *et al.* 2001; Augustesen *et al.* 2004; Karimpour and Lade 2010; Lade *et al.* 2010). Despite these studies, our understanding of sand creep and the accompanied permeability evolution over extended periods (months to years) remain poorly understood. Conclusions from short-term creep tests may not be readily extrapolated to the anticipated lifespan of tailings dams, especially when factoring in the enduring effects of delayed grain breakage.

To address these gaps, this letter reports a 450-day creep test on tailings sand, coupled with hydraulic conductivity measurements. The data is analysed using an integrated model that tracks the evolution of void-ratio, gradation, and hydraulic conductivity under sustained loads - an approach that has never been previously attempted due to the absence of comparable long-term hydro-mechanical data in the existing literature.

MATERIALS AND METHODS

This study uses tailings sand sourced from an active mine site, the same material used in Singh et al.

(2021). The grain size distributions (GSD) of the sample before and after the creep tests are measured using wet sieve analysis (ASTM 2017) (Fig. 1). The original tailings sand is classified as Silty Sand with e_{max} = 1.02, e_{min} =0.48, $\rho_{d,max}$ = 1830 kg/m^3 and $\rho_{d,min}$ = 1350 kg/m^3 (Singh et al. 2021). Insets in Fig. 1 show the X-ray scans of the sample before and after the creep test.

The high-stress permeability (HSP) cell originally developed by Singh et al. (2021) is adopted in the current study for the long-term creep test, as shown in Fig. 2a. The HSP cell can bear a maximum stress of 160 MPa and permits in-test measurement of hydraulic conductivity (k_s) without unloading the specimen. A pair of thin, 3-mm thick, stainless steel porous discs are placed at the top and bottom of the specimen to prevent fines loss and ensure uniform water pressure distribution.

The specimen is prepared to an initial void ratio of e_0= 0.57 (D_r= 83.4%) using wet pluviation method along with gentle tapping during multi-layer deposition to ensure uniform sample density (Bardet 1997). A unique design of this testing program is that we retrieved the in-situ pore water (referred to as tailings water from herein) that has already achieved equilibrium with the tailings from the active TSF after long-term exposure. The composition of the tailings water was characterized for major anions, elemental analysis, pH, and conductivity (see Table 2 in the Appendix A for the detailed chemical composition). The tailings water was used as both the saturating fluid and flushing fluid for the permeability tests to: (1) replicate the in-situ conditions as closely as possible, and (2) eliminate potential mineral dissolution effects, thereby preventing mass loss during repeated permeability tests.

The prepared sample is then mounted on a dead-weight loading system instrumented with a LVDT to record the vertical displacement of the loading cap (Fig. 2b, c). A vertical stress of 3 MPa which is equivalent to 200-m-high overburden with γ_d = 15 kN/m^3 (Obermeyer and Alexieva 2011) is applied at the top of the specimen. Although 3 MPa may seem low compared to the compressive strength of the constituent minerals (quartz, muscovite, plagioclase), high stress concentrations can still develop at grain contact points due to the angularity of the tailings sand grains (Singh et al. 2021). This localized stress amplification may lead to breakage mechanisms such as chipping, even at relatively low overall stress levels, leading to the generation of fines. Hydraulic conductivity (k_s) is periodically measured using the standard falling-head procedure (ASTM 2016a) with tailings water, conducted weekly in the first four months and then gradually

reduced to bi-monthly intervals.

TEST RESULTS

Fig. 3 reports the evolution of void ratio and hydraulic conductivity in the specimen. The test spanned a duration of 450 days, resulting in a final axial strain of ϵ_a = 8.22%. Notably, the specimen reached 80.1% of the final axial strain in the first minute, which aligns with the expected behaviour of coarse-grained soils. The subsequent creep contributed 19.9% to the total strain.

Inspecting the post-test GSD in Fig. 1, we can see that the gradation undergoes a subtle shift to the left, indicating a small amount of grain breakage. X-ray scans (Fig. 1) also revealed that particles exhibited a more angular shape after the creep test, possibly caused by intragranular fractures. The fines content of the specimen increased from 18.51% to 21.31% over 450 days under 200-m overburden. This amount of fines increase is not quite negligible given the duration of this test is only a fraction of the planed service life (typically 50 -100 years) of TSFs, and many existing ones have already exceeded or scheduled to raise beyond 200 m in height.

The initial k_s of the sample at unstressed state is measured to be 4.38 × 10^{-4} cm/s. The first in-test k_s measurement, conducted at 30 min, yielded a value of 2.35 × 10^{-4} cm/s. Subsequent permeability reduction is steady up to about 30 days. At around 30 days, the rate of k_s reduction becomes gradually accelerated, while no significant change of creep rate is observed. Eventually, k_s stabilized, reaching a final value of 1.51 × 10^{-5} cm/s by the conclusion of the test. While GSD and X-ray scanning (Fig. 1) suggest minor fine particle generation, this process typically occurs continuously throughout the creep stage, as evident in the creep strain curve. Thus, it is unlikely that the decline of k_s starting at around 30 days stems from pore clogging within the soil specimen. One possible explanation is that some fine particles within the specimen migrated downstream after several cycles of flushing and falling-head tests, forming a thin layer of fines deposited at the interface between the sample and the porous disc. This process manifested at around 30 days of creep and continued throughout the rest of the test. Another possible cause is the clogging of the stainless-steel porous disc itself. As shown in Table 2 in the Appendix A, the tailings water is relatively rich in ionic contents, and the stainless steel, although highly resistant to corrosion, may still slightly deteriorate

over time. Post-mortem examination of the porous disc showed slight signs of rusting but still perfectly permeable. Although it is difficult to pinpoint the exact cause of the accelerated reduction of k_s, we deemed that the hydraulic conductivity data after 30 days is more likely caused by changes in the testing system rather than that within the representative volume of the material. In the following section, the GSD data, the compression and creep data, and the early-stage (< 30 days) hydraulic conductivity data is be interpreted through an integrated constitutive framework.

MODEL INTERPREATION

The following workflow is adopted for integrated stress-strain-breakage-permeability prediction.

Mechanical wise, we have conducted single element test using the rate-dependent continuum breakage mechanics (CBM) theory to capture delayed breakage and compression of granular materials (Zhang and Buscarnera 2017). The model tracks the evolution of GSD via an internal variable *B* (Einav 2007a). The current GSD, $g_0(x)$, is computed by a linear interpolation $g(x) = (1 - B)g_0(x) + Bg_u(x)$ where $g_0(x)$ and $g_u(x)$ are the initial uncrushed and the ultimately crushed fractal GSDs with the following expressions:

$$g_0(x) = \frac{(3-\beta)x^{2-\beta}}{d_M^{3-\beta} - d_m^{3-\beta}}; g_u(x) = \frac{(3-\alpha)x^{2-\alpha}}{d_M^{3-\alpha} - d_m^{3-\alpha}} \quad (1)$$

where d_m and d_M are the minimum and maximum grain diameters, respectively; α and β determine the uniformity of the ultimate and initial GSDs, respectively. By defining a non-homogeneous flow potential and following the hyperplasticity procedure, a set of viscoplastic evolution laws similar to Perzyna (1966) can be defined for the rate-dependent CBM. The key components of the model are briefly described in Appendix B. The model parameters are calibrated based on the procedure described in (Zhang and Buscarnera 2017) and our past experience with similar tailings sand (Singh et al. 2021). They are listed in Table 1.

125 Table 1. Rate-dependent CBM Parameters

Elastic parameters	$\bar{K}$	980
	$\bar{G}$	1280
Yielding parameters	E_c (MPa)	0.35
	ω (deg.)	15
	M	1.2
Viscous parameters	n	15
	$\dot{B}_0$ (1/s)	10^{-5}
GSD parameter	β	2.0

126 The model is initially integrated under oedometric compression condition for the first 20 seconds to simulate
127 the process of incrementally adding deadweights to the loading frame. After reaching 3 MPa, the vertical
128 stress is fixed, and the system is allowed to continue evolve over time. The modelled and the measured
129 compression responses during the loading and creep stages are shown in Fig. 4a, demonstrating an overall
130 satisfactory agreement between the two. A slight underprediction of the creep strain is observed near the
131 end of the creep stage, as the model indicates a slowdown of the creep rate after around 100 days. Fig. 4b
132 shows that the predicted GSD evolution agrees well with measured ones, suggesting a small degree of
133 grain crushing occurred during the relatively low stress (3 MPa) creep test.

134 On the hydraulic side, six commonly used hydraulic conductivity models are chosen. They can be
135 generically expressed as (Vuković and Soro 1992):

136 $$k_s = \frac{g}{\nu} C\phi(n) d_e^2 \tag{2}$$

137 where k_s is the hydraulic conductivity; g is the gravitational acceleration; ν is the kinematic viscosity; C is
138 the dimensionless sorting coefficient; $\phi(n)$ is a function of porosity; d_e is the effective grain size diameter.
139 The expressions of C, $\phi(n)$ and d_e for the six models are summarized in Singh et al. (2021). These models
140 are integrated with rate-dependent CBM as follows: CBM simulates stress, strain, porosity, and breakage
141 B, which updates the GSD and characteristic grain sizes like d_{10} and d_{20}. These values are then feed to
142 Eq. (2) to predict hydraulic conductivity of the specimen over time.

143 Fig. 5 shows the comparison between the measured permeability and the predictions made by all six
144 hydraulic models. Note that all mechanical parameters for CBM have already been calibrated and are fixed
145 as in Table 1, and there are no tuneable parameters in the hydraulic conductivity models. The comparison

shown in Fig. 5 therefore shows the true predictions from the coupled hydraulic models and CBM. It is found that the Kozeny-Carman and Terzaghi models provide the closest agreement with the experimental results for the time until 30 days. They also capture the initial rapid permeability reduction due to compression and the slower decrease from void collapse and fines generation during creep, demonstrating their effectiveness for tailings sand subjected to both instantaneous loading and long-term effects. The USBR and Breyer models overpredict the hydraulic conductivity approximately by a factor of 2, while the Slitcher model slightly underpredicts. As similarly noted in Singh et al. (2021), the Hazen model significantly underpredicts the hydraulic conductivity by several orders of magnitude.

CONCLUDING REMARKS

This study delves into the intricate evolution of creep and hydraulic conductivity in tailings material subjected to sustained stresses. A novel HSP cell is adopted for combined oedometric compression and in-test permeability measurements. The 450-day creep test showed that primary consolidation concluded within the first minute as expected for sand. Subsequent creep accounts for around 19.9% of the total compressive strain. Hydraulic conductivity exhibited around 20% decrease at the early stage (0-30 days) which reflects the evolution of intrinsic permeability of the tailings sand, followed by another decline at the later stage which is likely a characteristic of the testing system. Pre- and post-experiment gradation and X-ray scanning shows notable particle breakage and contact abrasion, accompanied with a 2.8% increase in fines content. The GSD, compression, and hydraulic conductivity (< 30 days) are interpreted through the rate-dependent CBM model combined with six hydraulic conductivity models. We found that the Kozeny-Carman and Terzaghi model offered the most accurate predictions, while the Hazen and Slitcher model underestimated and the Breyer and USBR model overestimated the hydraulic conductivity evolution. These findings align with our prior conclusions. The current study showcases the capacity of the HSP cell and the integrated CBM model for understanding the stress-strain-hydraulic conductivity response of sands at both loading and creep stages, offering new insights into tailings material behaviour at in-situ conditions

Our experimental results underscore the importance of continuously monitoring the internal structure of soil samples during long-term, combined stress and flow tests. Repeated flushing under sustained high stress may induce fines migration, potentially affecting the measured global hydraulic conductivity at the later

stage of the test. Future enhancements to the test setup could include developing a miniaturized X-ray transparent HSP cell, enabling in-test micro-CT imaging to track fines distribution, grain crushing, and contact morphology evolution throughout extended creep tests. In addition to this, although the 450-day duration far exceeds conventional timelines of the experiments reported in the literature, it still represents a small fraction of the operational lifespan of tailings storage facilities (TSFs), which typically span several decades. Extrapolation of these results to longer time scales must therefore be approached with caution.

Conflicts of Interest

The authors have no conflict of interest.

Data Availability Statement

Some or all data, models, or code that support the findings of this study are available from the corresponding author upon reasonable request.

Acknowledgements

Yida Zhang wishes to acknowledge the support of U.S. National Science Foundation under Award Number 2237332 and U.S. Department of Energy under Award Number DE-SC0024391. We are also grateful to Amanda Adams at Stantec Inc. for her assistance in providing testing materials and project support.

LIST OF NOTATIONS

$e_{\min}$, e_{max}	Minimum and maximum void ratio
$\rho_{\min}$, ρ_{max}	Minimum and maximum density
k_s	Hydraulic conductivity
e_0	Initial void ratio
γ_d	Dry unit weight
ϵ_a	Axial Strain
$g_0(x), g_u(x)$	Initial and ultimate GSD function
B	Breakage index
d_m , d_M	Minimum and maximum grain diameters
α , β	Uniformity parameters for initial and ultimate GSDs
g	Gravitational acceleration
ν	Kinematic viscosity

C	Dimensionless sorting coefficient
$\phi(n)$	Porosity function
d_e	Effective grain size diameter
$E_c, n, \dot{B}_0, \omega, M$	VBM Model parameters
E_B	Breakage energy
ζ_{pB}	Overstress function
p, q	Mean and deviatoric stresses
$\epsilon_v^p, \epsilon_s^p$	Plastic volumetric and deviatoric strain

189

REFERENCES

Abraham, M. R. and Susan, T. B. (2017). Water contamination with heavy metals and trace elements from Kilembe copper mine and tailing sites in Western Uganda; implications for domestic water quality. *Chemosphere.* **169**, No. 281-287. https://doi.org/10.1016/j.chemosphere.2016.11.077

ASTM (2016a). Standard test method for measurement of hydraulic conductivity of porous material using a rigid-wall, compaction-mold permeameter. ASTM.

ASTM (2017). Standard Test Methods for Determining the Amount of Material Finer than 75-μm (No. 200) Sieve in Soils by Washing. ASTM International.

Augustesen, A., Liingaard, M. and Lade, P. V. (2004). Evaluation of time-dependent behavior of soils. *International Journal of Geomechanics.* **4**, No. 3, 137-156. https://doi.org/10.1061/(ASCE)1532-3641(2004)4:3(137)

Bardet, J.-P. (1997). Experimental soil mechanics. Prentice Hall.

Barrera, S., Valenzuela, L. and Campaña, J. (2011). Sand tailings dams: design, construction and operation. Proceedings Tailings and Mine Waste. Vancouver, BC. https://dx.doi.org/10.14288/1.0107705

Eaton, A. D., Franson, M. A. H., Association, A. P. H., Association, A. W. W. and Federation, W. E. (2005). Standard Methods for the Examination of Water and Wastewater. American Public Health Association.

Einav, I. (2007a). Breakage mechanics—part I: theory. *Journal of the Mechanics and Physics of Solids.* **55**, No. 6, 1274-1297. https://doi.org/10.1016/j.jmps.2006.11.003

Einav, I. and Puzrin, A. M. (2004). Pressure-dependent elasticity and energy conservation in elastoplastic models for soils. *Journal of Geotechnical and Geoenvironmental engineering.* **130**, No. 1, 81-92. https://doi.org/10.1061/(ASCE)1090-0241(2004)130:1(81)

Houlsby, G. and Puzrin, A. (2006). Principles of hyperplasticity: an approach to plasticity theory based on thermodynamic principles. Springer London. https://doi.org/10.1007/978-1-84628-240-9.

Karimpour, H. and Lade, P. V. (2010). Time effects relate to crushing in sand. *Journal of Geotechnical and Geoenvironmental Engineering.* **136**, No. 9, 1209-1219. https://doi.org/10.1061/(ASCE)GT.1943-5606.0000335

Lade, P. V., Nam, J. and Liggio Jr, C. D. (2010). Effects of particle crushing in stress drop-relaxation experiments on crushed coral sand. *Journal of Geotechnical and Geoenvironmental Engineering.* **136**, No. 3, 500-509. https://doi.org/10.1061/(ASCE)GT.1943-5606.0000212

Leung, C. F., Lee, F. H. and Yet, N. S. (1996). The role of particle breakage in pile creep in sand. *Canadian Geotechnical Journal.* **33**, No. 6, 888-898. https://doi.org/10.1139/t96-119

Obermeyer, J. and Alexieva, T. (2011). Design, construction and operation of a large centerline tailing storage facility with high rate of rise. Proceedings Tailings and Mine Waste. Vancuover, BC. https://dx.doi.org/10.14288/1.0107726

Perzyna, P. (1966). Fundamental problems in viscoplasticity. *Advances in applied mechanics.* **9**, No. 243-377. https://doi.org/10.1016/S0065-2156(08)70009-7

Riemer, M., Moriwaki, Y. and Obermeyer, J. (2008). Effect of high confining stresses on static and cyclic strengths of mine tailing materials. https://doi.org/10.1061/40975(318)64

Santamarina, J. C., Torres-Cruz, L. A. and Bachus, R. C. (2019). Why coal ash and tailings dam disasters

occur. *Science.* **364**, No. 6440, 526-528. https://doi.org/10.1126/science.aax1927

Singh, S., Zurakowski, Z., Dai, S. and Zhang, Y. (2021). Effect of grain crushing on the hydraulic conductivity of tailings sand. *Journal of Geotechnical and Geoenvironmental Engineering.* **147**, No. 12, 04021143. https://doi.org/10.1061/(ASCE)GT.1943-5606.0002667

Takei, M., Kusakabe, O. and Hayashi, T. (2001). Time-dependent behavior of crushable materials in one-dimensional compression tests. *Soils and foundations.* **41**, No. 1, 97-121. https://doi.org/10.3208/sandf.41.97

Valenzuela, L. (2016). Design, construction, operation and the effect of fines content and permeability on the seismic performance of tailings sand dams in Chile. *Obras y proyectos.* No. 19,

Vuković, M. and Soro, A. (1992). Determination of hydraulic conductivity of porous media from grain-size composition. Water Resources Publications.

Yolcubal, I., Demiray, A. D., Çiftçi, E. and Sanğu, E. (2016). Environmental impact of mining activities on surface water and sediment qualities around Murgul copper mine, Northeastern Turkey. *Environmental Earth Sciences.* **75**, No. 1-25. https://doi.org/10.1007/s12665-016-6224-y

Zhang, Y. and Buscarnera, G. (2017). A rate-dependent breakage model based on the kinetics of crack growth at the grain scale. *Géotechnique.* **67**, No. 11, 953-967. https://doi.org/10.1680/jgeot.16.P.181

APPENDIX A: CHEMICAL ANALYSIS OF THE TAILINGS WATER

Anion concentrations were measured using ion chromatography (ICS-6000, Thermo Scientific) following Standard Method 4110B (Eaton *et al.* 2005). For elemental analysis, the tailing water was filtered (0.45 μm) prior to acidification to quantify dissolved concentrations with inductively coupled plasma-mass spectrometry following EPA method 6020B. The chemical composition of the tailings water is presented in Table 2. The tailing water had an alkaline pH (8.1) and moderately high salinity as indicated by conductivity (3.03 mS/cm). Using Visual MINTEQ to model the composition, the tailings water composition is near saturation for calcium sulfate precipitation (saturation index -0.25 for gypsum). The analysis also revealed that the in-situ water has moderate concentrations of trace metals (e.g., arsenic, copper, manganese, and nickel), which is consistent with tailing water from other copper mines (Yolcubal *et al.* 2016; Abraham and Susan 2017).

Table 2. Chemical Composition of the in-situ tailings water

Constituent	Units	Value	Constituent	Units	Value
Conductivity	mS/cm	3.03	Cadmium[1]	µg/L	< 1.0
pH	–	8.1	Chromium[1]	µg/L	< 3.0
Sodium[1]	mg/L	276	Cobalt[1]	µg/L	< 1.0
Calcium[1]	mg/L	322	Copper[1]	µg/L	74.6
Potassium[1]	mg/L	84.0	Iron[1]	µg/L	< 100.0
Magnesium[1]	mg/L	12.2	Lead[1]	µg/L	< 0.2
Chloride[2]	mg/L	343	Manganese[1]	µg/L	56.6
Sulfate[2]	mg/L	1001	Nickel[1]	µg/L	33.4
Nitrate+Nitrite[2]	mg/L as N	9.5	Selenium[1]	µg/L	< 3.0
Bromide[2]	mg/L	0.843	Strontium[1]	µg/L	2018
Aluminum[1]	µg/L	< 10.0	Uranium[1]	µg/L	< 0.2
Arsenic[1]	µg/L	13.8	Vanadium[1]	µg/L	10.8
Barium[1]	µg/L	66.4	Zinc[1]	µg/L	131.8

[1]Dissolved elemental concentration by inductively coupled plasma-mass spectrometry
[2]Anion concentration by ion chromatography

APPENDIX B: VISCOPLASTIC BREAKAGE MODEL (VBM)

Following the hyperplasticity procedure (Houlsby and Puzrin 2006) and using a non-homogenous flow potential *w* defined for the CBM model in (Zhang and Buscarnera 2017), the inelastic evolution laws can be defined for the rate-dependent CBM:

$$\dot{B} = \dot{B}_0 cos^2 \omega \zeta_{pB}^{n/2}$$

$$\dot{\epsilon}_v^p = \frac{\dot{B}_0 E_B}{p} sin^2 \omega \zeta_{pB}^{n/2} \qquad (B.1)$$

$$\dot{\epsilon}_s^p = \frac{\dot{B}_0 E_B}{p} \frac{\dot{B}_0 E_c}{(1-B)^2} \frac{q}{M^2 p^2} sin^2 \omega \zeta_{pB}^{n/2}$$

where E_c is the critical breakage energy that controls the onset of breakage; *n* and $\dot{B}_0$ are corrosion index and reference breakage rate, respectively; ϵ_v^p, ϵ_s^p are the plastic volumetric and deviatoric strain; *p, q* are the mean and deviatoric stresses; E_B is the breakage energy; ω is a constant controlling the coupling between plastic compaction and grain breakage; *M* the critical stress ratio; ζ_{pB} the overstress function (Perzyna 1966):

$$\zeta_{pB} = \left\langle \frac{(1-B)^2 E_B}{E_c} + \left(\frac{q}{Mp}\right)^2 - 1 \right\rangle \qquad (B.2)$$

No inelastic flow will occur when $\boldsymbol{\zeta_{pB} = 0}$, which defines the model's yield surface. The model is completed by adopting a pressure-dependent elastic relation (Einav and Puzrin 2004).

LIST OF FIGURES

Figure 1. Grain size distribution of the uncrushed (before creep) and crushed (after creep) underflow tailings sand; The insets show the X-ray scanning of tailings material before and after creep test.

Figure 2. (a) HSP cell and its cross-sectional view showing internal components (modified after Singh et al. (2021)); (b) test setup for combined compression and hydraulic conductivity measurements; (c) assembled specimen with an initial radius of 28 mm and height of 30.8 mm in HSP cell under load.

Figure 3. Evolution of void ratio and hydraulic conductivity of the specimen during the creep test.

Figure 4. Comparison of (a) mechanical response (b) GSD between the experimental data and the calibrated rate-dependent CBM for the 450-day creep tests; B=0.0691 is the breakage index after a 450-day creep stage.

Figure 5. Comparison between the experimental data for long-term creep test and predictions from the six hydraulic models coupled with the rate-dependent CBM model. The transparent data indicates hydraulic conductivity data after 30 days.

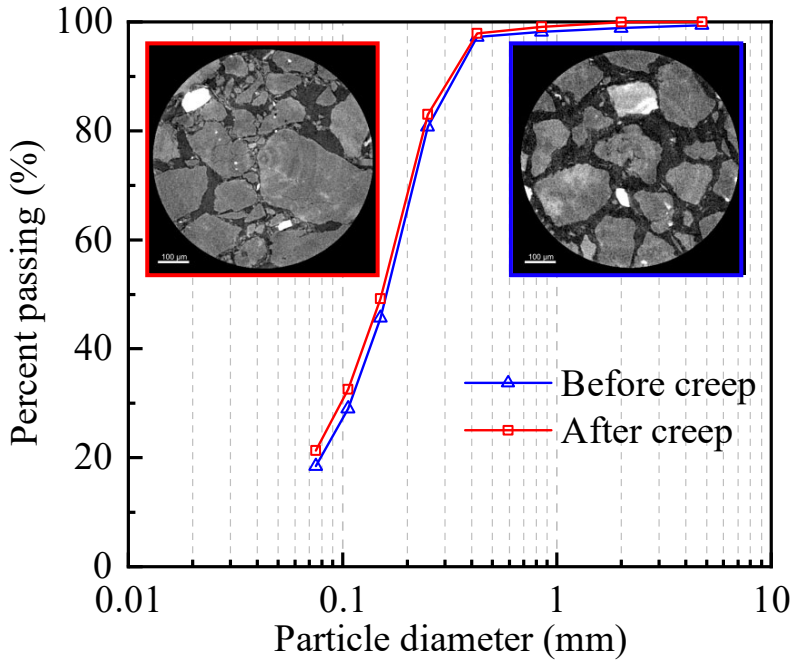

310

311 Fig. 1. Grain size distribution of the uncrushed (before creep) and crushed (after creep) underflow tailings

312 sand; The insets show the X-ray scanning of tailings material before and after creep test.

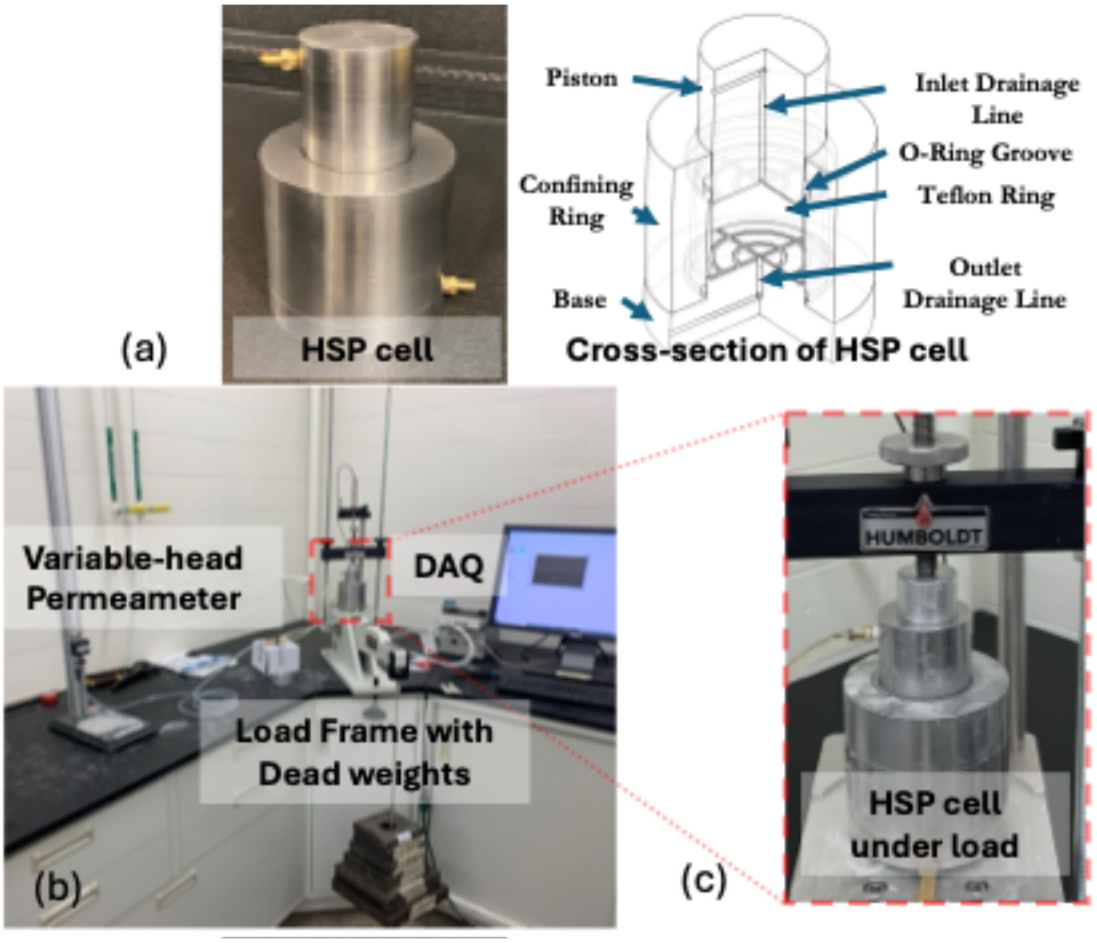

313

314 Fig. 2. (a) HSP cell and its cross-sectional view showing internal components (modified after Singh et al.

315 (2021)); (b) test setup for combined compression and hydraulic conductivity measurements; (c)

316 assembled specimen with an initial radius of 28 mm and height of 30.8 mm in HSP cell under load.

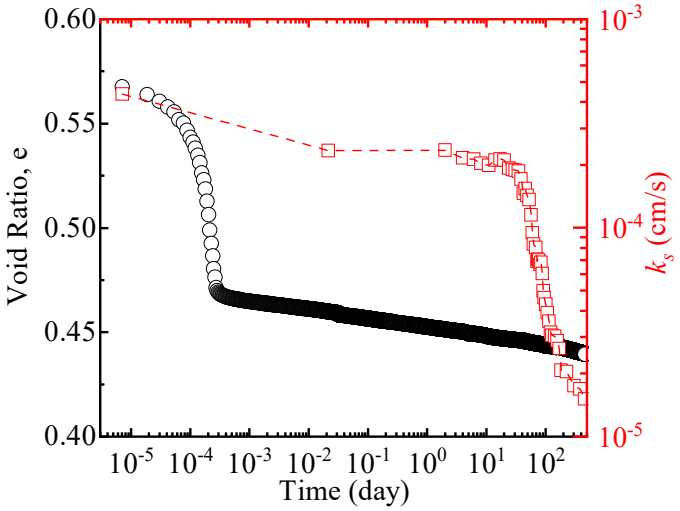

317

318 Fig. 3. Evolution of void ratio and hydraulic conductivity of the specimen during the creep test.

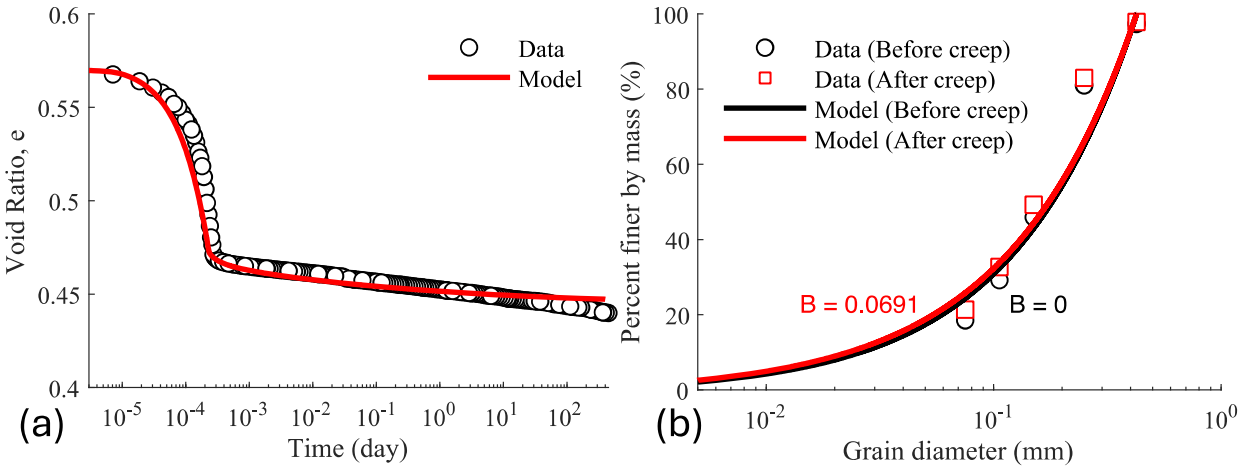

Fig. 4. Comparison of (a) mechanical response (b) GSD between the experimental data and the calibrated rate-dependent CBM for the 450-day creep tests; B=0.0691 is the breakage index after a 450-day creep stage.

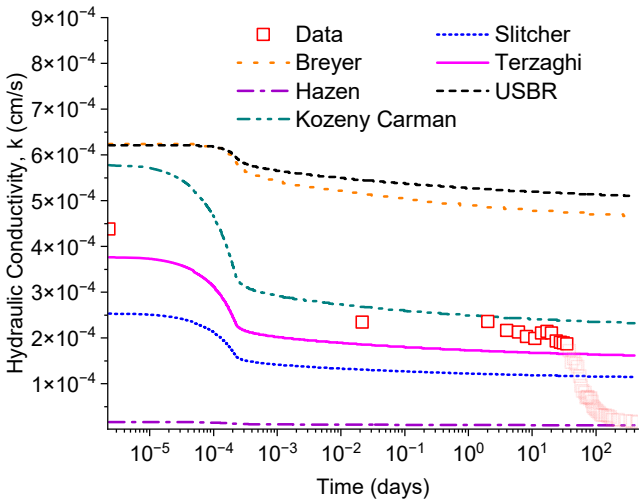

323

324 Fig. 5. Comparison between the experimental data for long-term creep test and predictions from the six

325 hydraulic models coupled with the rate-dependent CBM model. The transparent data indicates hydraulic

326 conductivity data after 30 days.